Siège: Genève, Suisse Seat: Geneva, Switzerland

ORGANISATION EUROPÉENNE POUR LA RECHERCHE NUCLÉAIRE

EUROPEAN ORGANIZATION FOR NUCLEAR RESEARCH

Laboratoire Européen pour la Physique des Particules

European Laboratory for Particle Physics

Technical Inspection and Safety Commission

CERN-TIS/2000-009/GS

Simulations of argon accident scenarios in the ATLAS experimental cavern: a safety analysis

Fabrizio Balda and Marc Vadon

ABSTRACT

Some characteristic accidents in the ATLAS experimental cavern (UX15) are simulated by means of STAR-CD, a code using the "Finite-Volume" method. These accidents involve different liquid argon leaks from the barrel cryostat of the detector, thus causing the dispersion of the argon into the Muon Chamber region and the evaporation of the liquid. The subsequent temperature gradients and distribution of argon concentrations, as well as their evolution in time are simulated and discussed, with the purpose of analysing the dangers related to asphyxiation and to contact with cryogenic fluids for the working personnel. A summary of the theory that stands behind the code is also given. In order to validate the models, an experimental test on a liquid argon spill performed earlier is simulated, showing that the program is able to output reliable results. At the end, some safety-related recommendations are listed.

Geneva, Switzerland
June 2000

Table of Contents

1 Safety problems in the ATLAS experimental cavern

The ATLAS detector will be located about 100 m underground in the experimental cavern UX15 (Fig. 1), which will also have to contain lots of auxiliary installations, related to electronic, detection, cryogenic and safety systems.

The detector will contain three cryostats (one barrel and two end-caps) full of high purity liquid argon (45 m^3 in the barrel and 19 m^3 in each end-cap). This will be kept to the approximately constant temperature of about 90 K, and the gas-liquid interface in the overflow vessel will be at 1.25 bar abs. in normal conditions. A large number of feedthroughs will be inserted into the cryostat: some of them will contain various types of sensors, while others will work as cryo-lines for liquid or gas, for filling or emptying purposes. These feedthroughs, placed in-between the cold and warm vessel, must be vacuum-sealed and each will be equipped with its own vacuum volume, so that the main vacuum will not be damaged even in the case of a leak.

The cryogenic system in UX15 will also comprise heat exchangers, three overflow vessels for argon, monitoring systems for temperature, pressure and liquid level, safety system lines (safety valves, draining pipes), pumping systems for LAr[i], storage vessels for LAr and LN, circulating plants for cryogenic liquids, and cooling-down and warming-up units. A special system of *flexible cryo-lines* will allow opening and displacement of the end-caps during maintenance periods.

Inside UX15 there will be some hazards related to the use of argon as a cryogenic liquid inside the ATLAS cryostat. These hazards will be essentially that of asphyxiation and injuries as a result of the low temperature in the case of a leakage or a severe accident. Argon is not dangerous itself as it is an inert, non-toxic, non-flammable gas; nevertheless, if its concentration should reach high values, the amount of available oxygen for a human being could decrease beyond a critical value. In particular, if oxygen concentration, normally at 21% in volume, goes below 17%, man begins to show slower reaction times. Around 10% there's a loss of consciousness, and between 8% and 4% human beings can suffer severe damage. Besides, the temperature at which argon is stored (90 K) will be, in the case of a release, a significant source of frostbite, cryo-burns, hypothermia, and other forms of cold-related injuries. Similarly, the damage that could result to structures and equipment impinged upon is not negligible ([1], [2], [3], [4], [5], [6], [7]).

[i] LAr stands for "liquid argon", LN for "liquid nitrogen".

2 Objectives of the work

The main purpose of this work is to try to perform a simulation of some possible accident scenarios, involving different amounts of argon, and to evaluate the consequences for working personnel who will eventually be present in the cavern. We want to obtain credible orders of magnitude of gas concentration, temperature distribution and characteristic times of the considered accidents, in order to estimate the effectiveness of safety systems. Useful information could also be obtained for the realization of a valid evacuation plan, which still does not exist. In addition, we want to verify the functioning of the ventilation system - according to the status of the project - and evaluate the “weight” of natural convection on the global flow field, that is to say the influence that temperature differences, heating and cooling can have upon the motion of fluid.

In order to validate the chosen models and all hypotheses, we’ll try to reproduce the results of a LAr spill test from a pressurized vessel ([8]). This section will also be of help in getting useful information for the realization of a future experiment, which is planned.

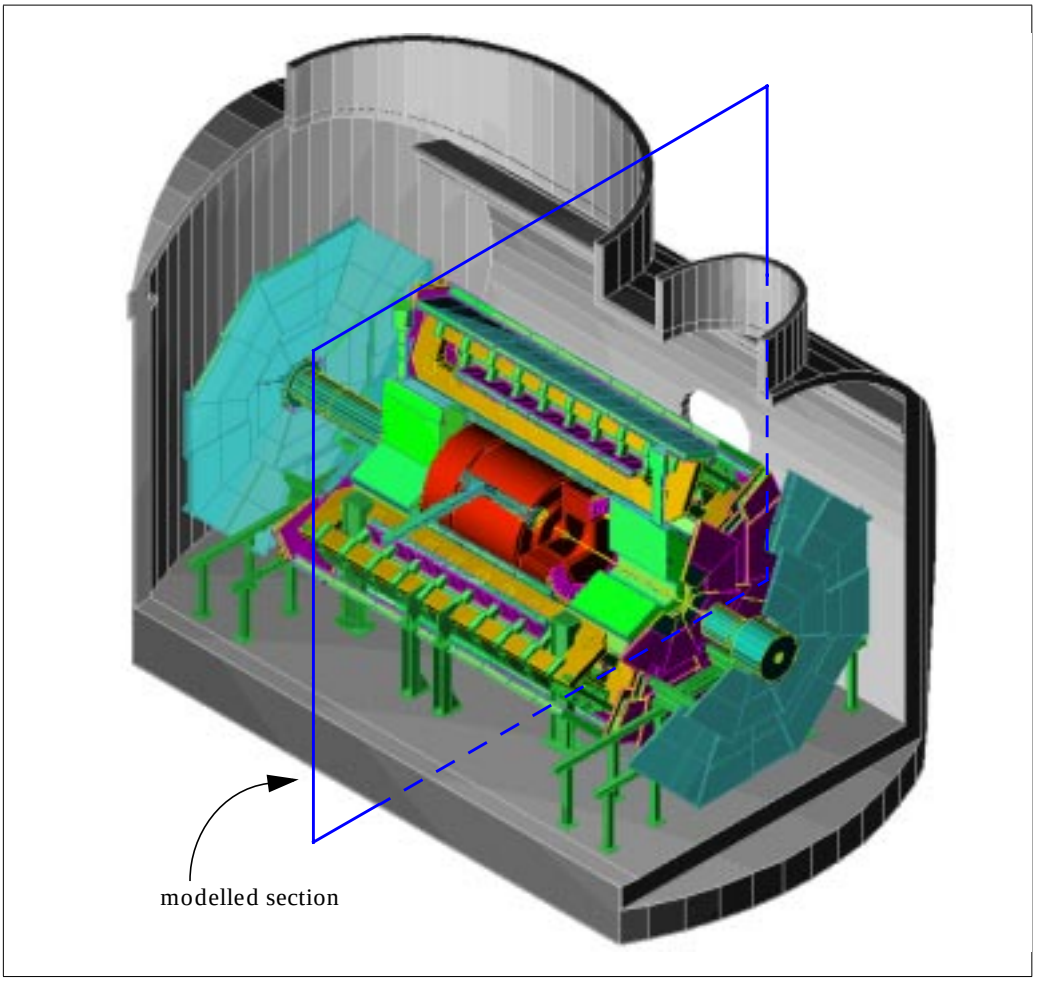

Figure 1 3D-view of the ATLAS detector and of the experimental cavern

3 Simulation results

The modelling of the normal running situation has pointed out the importance of natural convection (Gr/Re^2 >>1)[ii]: it acts significantly above all of the variables and physical properties, therefore it cannot be neglected. The most interesting field is the one related to temperature (Fig. 2), in which one can note that the maximum ΔT is around 5-10°C, not far from the previsions of some preliminary studies. Note that in this simulation the ventilation system is assumed to work at 100% of its capacity (both for air insertion and mixture extraction) and is able to extract 100 kW of thermal load.

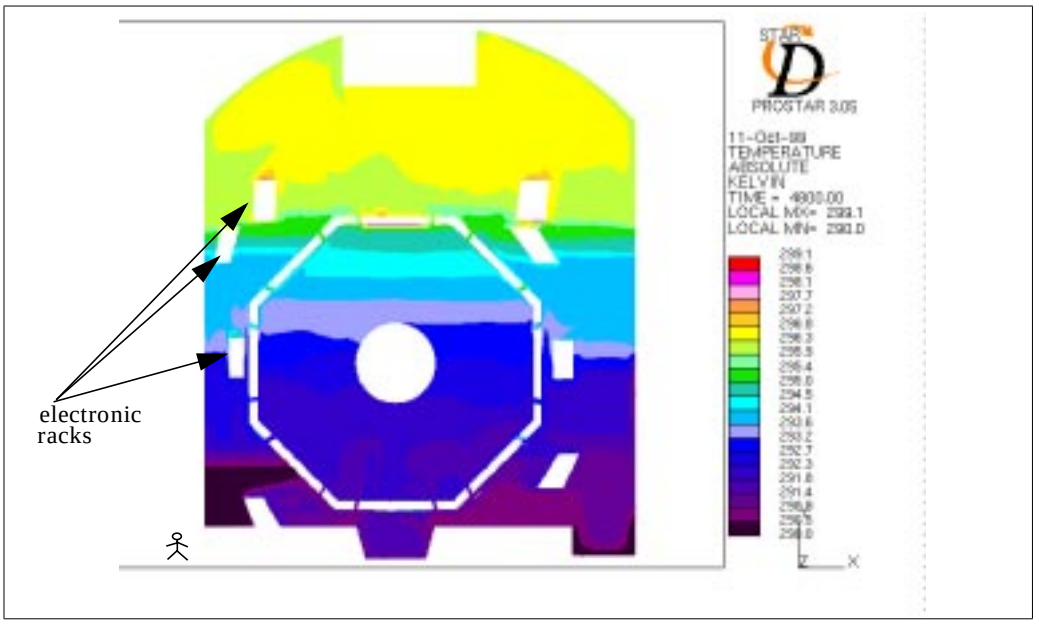

Figure 2 Temperature field during normal running (regime)

The flow motion can be classified as globally turbulent (or at least in the laminar-turbulent transition region) even if the velocity values are low (< 1 m/s): this comes out from a brief analysis of the dimensionless groups ($Gr*Pr >> 10^9$)[iii].

The considered model represents only the external layer of muon chambers, but the results were not significantly affected by this choice. The modelling of a regime situation in which the ventilation system does not work at all shows a slightly more chaotic behaviour in all of the fields (temperature, velocity, density, etc.) than before, even after a long time (1h 20'). This highlights the "stabilizing" function of such a system.

We simulated three different accidents:

- **Complete breakdown of a feedthrough;**
- **Argon leak through a weld/seal due to structural failure or poor**

[ii] *Gr* = Grashof number; *Re* = Reynolds number; *Pr* = Prandtl number.
[iii] See note 2.

maintenance (without internal overpressure);

- **Argon leak through a weld/seal due to internal overpressure.**

In all cases the rupture is supposed to take place in the lowest point of the cryostat, where the absolute pressure is maximum; here the release allows diffusion of the gas in the low zones of the cavern, where the majority of working personnel are likely to be located. We will always refer to the barrel, where the largest quantity of argon will be stored, and we will consider simultaneous ruptures in the barrel and in the end-caps as non credible. Finally, in each accident scenario, we will assume the flow rate of the ventilation system to be double the normal rate, as foreseen in the project specifications ([9]).

The first situation corresponds to a catastrophic scenario and involves a total structural failure of a feedthrough, possibly due to the loss of control of an operating crane (probably because of human error) during a maintenance period. Although it is a very unlikely event, we want to underline the fact that this accident is more likely to occur when cavern UX15 is full of people working than during normal running, when nobody will be present. Figure 3 shows temperature and argon weight concentration distributions 1 minute after the beginning of the accident (rupture section ~13 cm, release flow rate ~184 l/s). The scale aims to emphasize the consequences of the accident ([10]).

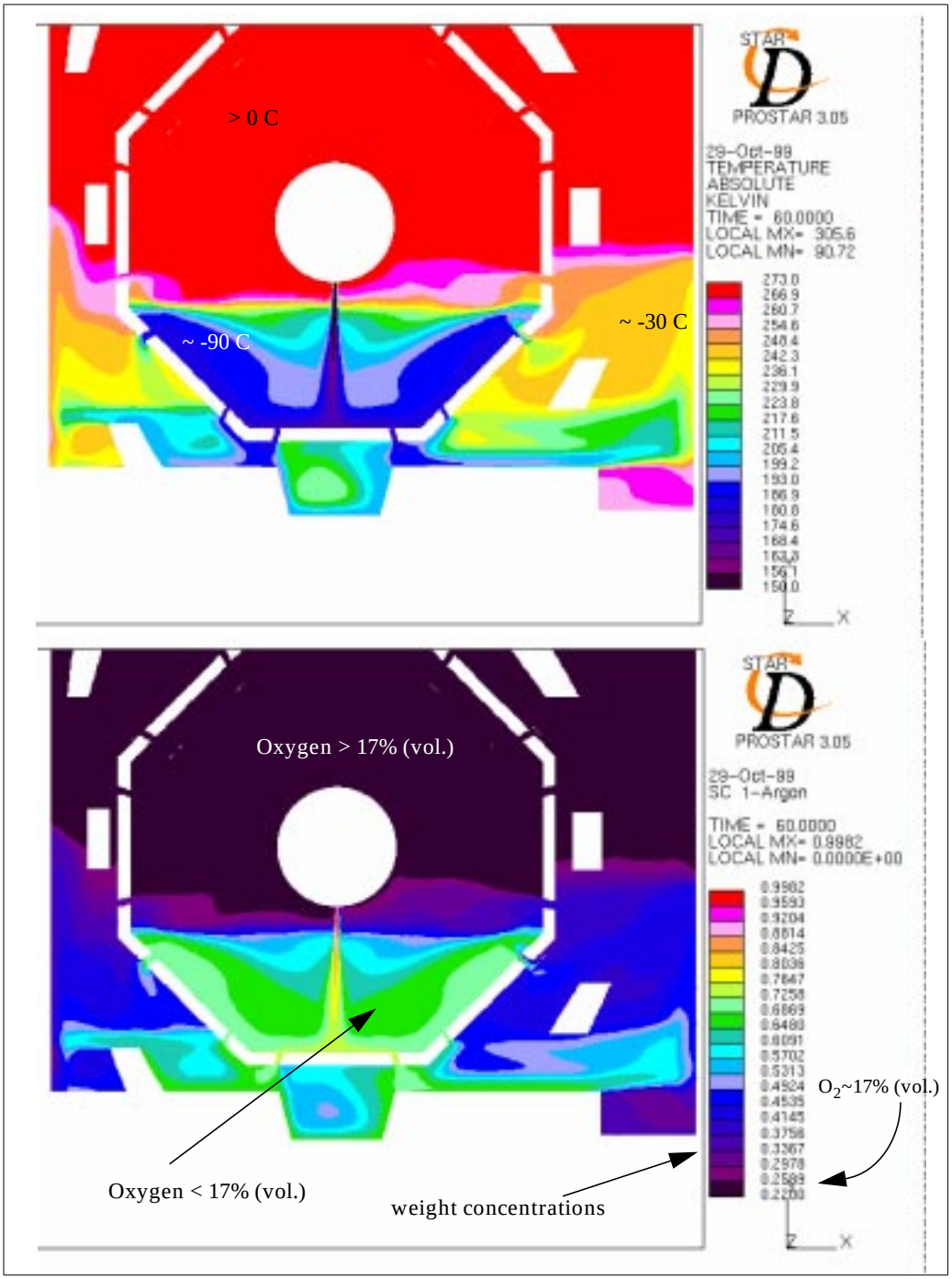

Figure 3 Temperature and argon concentration distributions 1 minute after the beginning of the release (complete breakdown of a feedthrough)

The two graphics of Figure 3 highlight the zones in which the temperature falls below 0° C and the oxygen concentration decreases below 17% in volume (thus corresponding to an argon weight concentration of approximately 25%). Although this is the “most dangerous” section of the whole cavern and all of the hypotheses are conservative, the situation seems extremely critical for anybody located in UX15 at the moment of the accident. Consequences can be serious: the cloud which is suddenly formed constitutes an obstacle to movement (this phenomenon is also enhanced by the fact that the dew point is at $12°C$), and the dramatic temperature drop can provoke serious injuries to all people working in the proximity of the

rupture point, especially in the lowest zones. It seems that the temperature-related sources of harm are more dangerous than breathing high concentrations of gas. The evacuation of the cavern is expected to be possible in a short time, and we can reasonably state that a large number of workers (especially those located in the extreme parts of the cavern) will be able to reach safe zones without significant consequences to their health.

The simulations of the two leakages (i.e. with and without internal pressure rise) have given quite similar results, and the second one was realized with the help of a more precise geometry than was previously used (representing all of the three layers of muon chambers) in order to show that further complications of the model do not significantly change the output and result in exactly the same orders of magnitude of all variables. This is also due to the fact that the internal pressure at the liquid-gas interface of the overflow vessel will rise to only 1.7 bar abs., before a safety valve opens and avoids further overpressures.

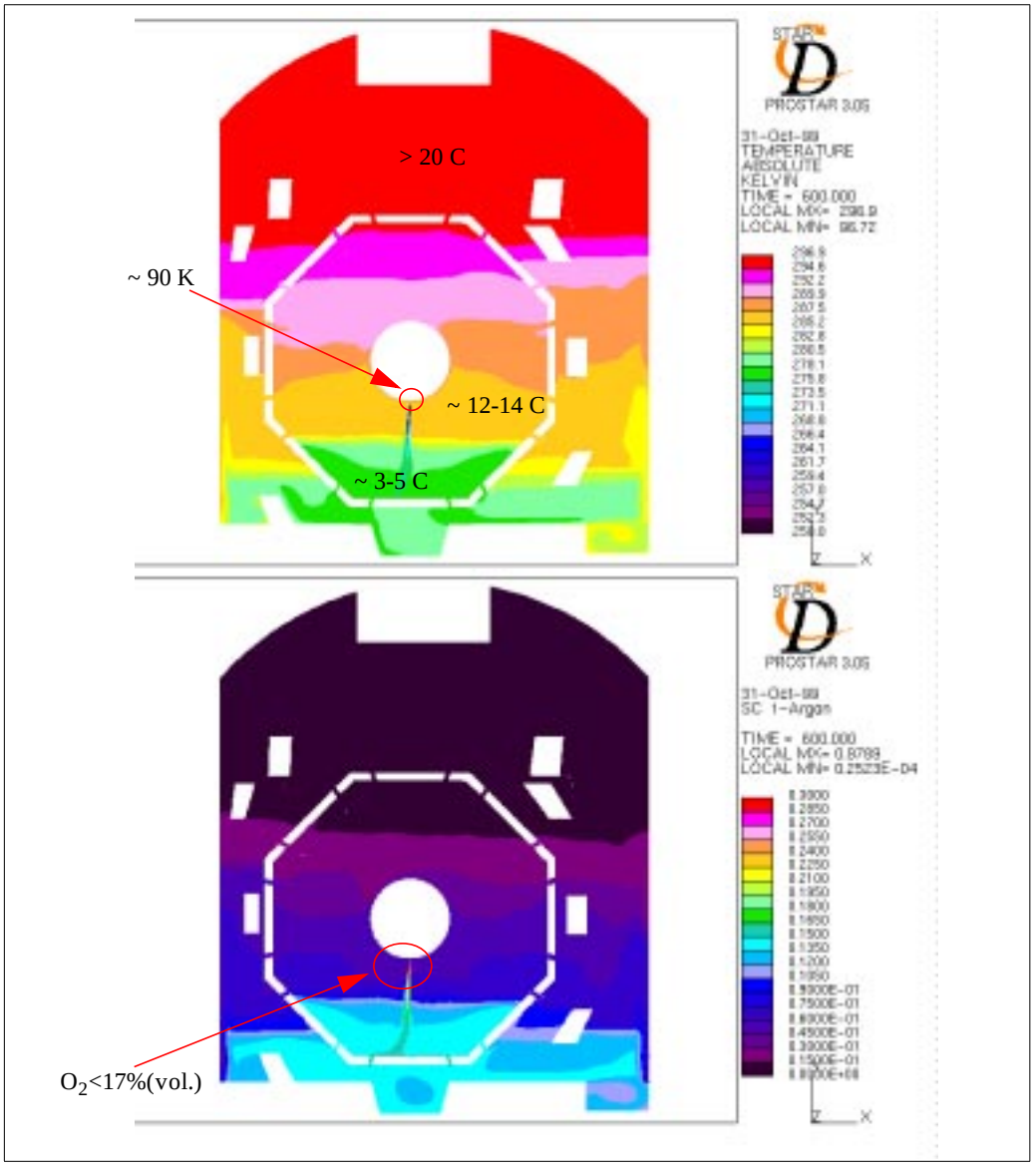

Figure 4 Temperature and argon concentration distribution after 10 minutes (leak without internal overpressure)

In Figures 4 and 5, temperature and argon weight concentration in UX15 10 minutes after the beginning of the release are shown for the two accidents considered; the scales have been carefully chosen to better visualize the situation (note that the fact that the minimum reported temperature is 200K or 250 K simply means that the last value in the scale indicates *all of the domain zones* at $T \leq 200K$ or, respectively, 250 K). The chosen rupture section has a length of 17.3 mm, corresponding to a release flow rate of 3.28 l/s in the first situation (no internal overpressure) and of 3.8 l/s in the second one (internal overpressure).

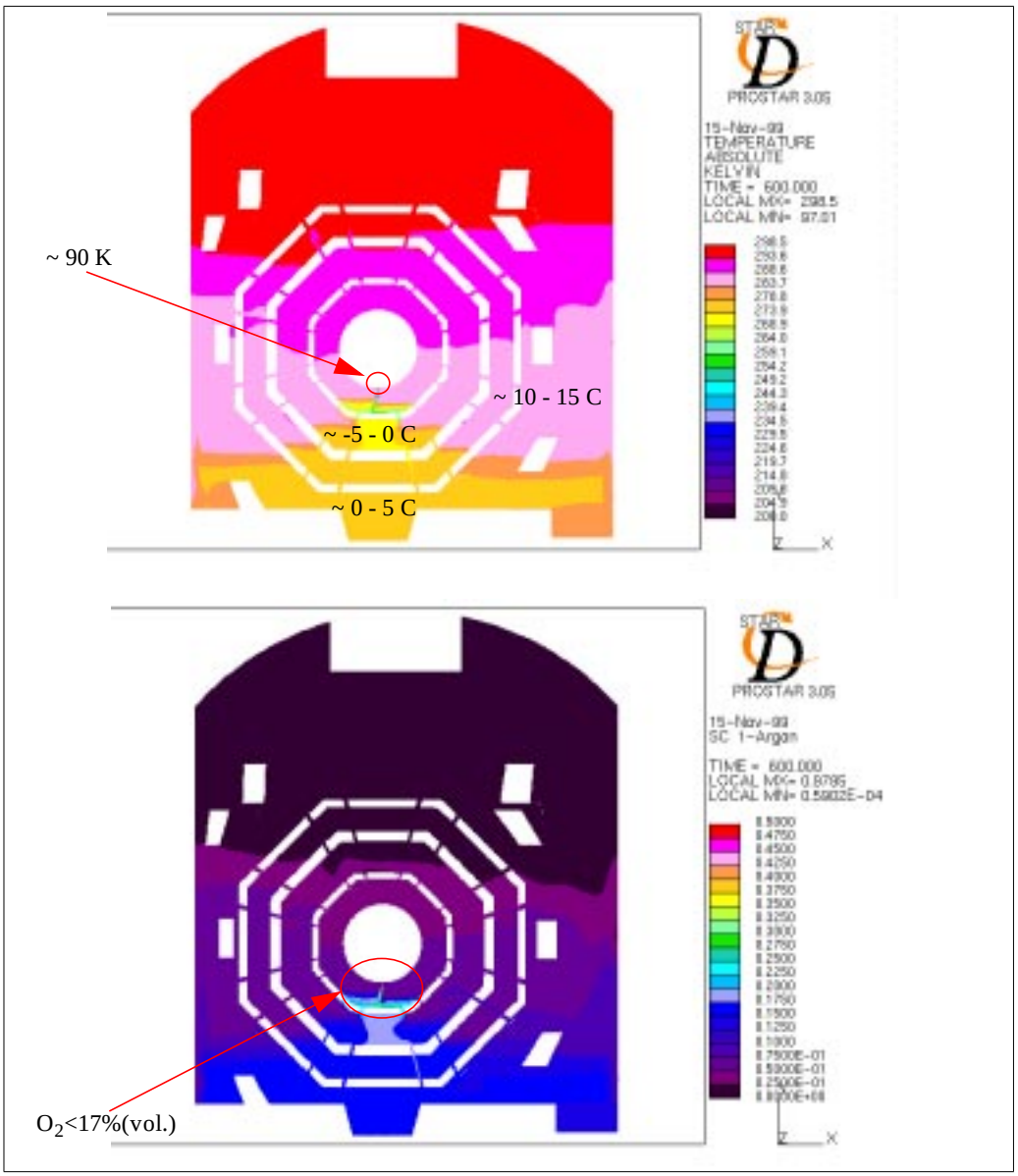

Figure 5 Temperature and argon weight concentration 10 minutes after the beginning of the release (leak with internal overpressure)

In both cases, it is evident that the danger of serious harm only exists for people who will be located very close to the rupture point at the moment of the accident. This is rather unlikely to happen. The most relevant obstacle to

any escape is again represented by the dense cloud which is rapidly formed. The movements of working personnel, already made difficult by the limited available space and by the large number of installations, will be further hindered, and low visibility may cause minor or even serious injuries and lead to panic. Any personnel training and evacuation plan should take these factors into account. The significant decrease of temperature could create some additional problems, while it seems that concentrations of argon will not constitute a serious danger. We can reasonably conclude that this kind of accident might evolve in more serious scenarios, but the probability of dramatic consequences for people is very low. It is likely that all of the workers located in zones within UX15 which are not under the region of the rupture point will be able to reach safe areas without difficulties.

Smaller argon leaks should not be a serious source of risk for personnel. At the end of this paper a short summary of the main safety recommendations related to the considered accidents is given ([11], [12], [13], [14], [15]).

4 Simulation of an experiment

We must now try to validate our model and all the techniques we used in the ATLAS simulations. This task can be accomplished by means of the simulation of an experiment ([8]): making use of the data about the conditions in which the experiment was carried out and implementing the correct physical models into Star-CD, it is possible to get a set of results to be compared with the experiment. We will make sure, wherever possible, that the hypothesis and assumptions we made before are left unchanged.

This section also has a second purpose, that is to develop information on the behaviour of vaporizing argon, about which very little literature currently exists.

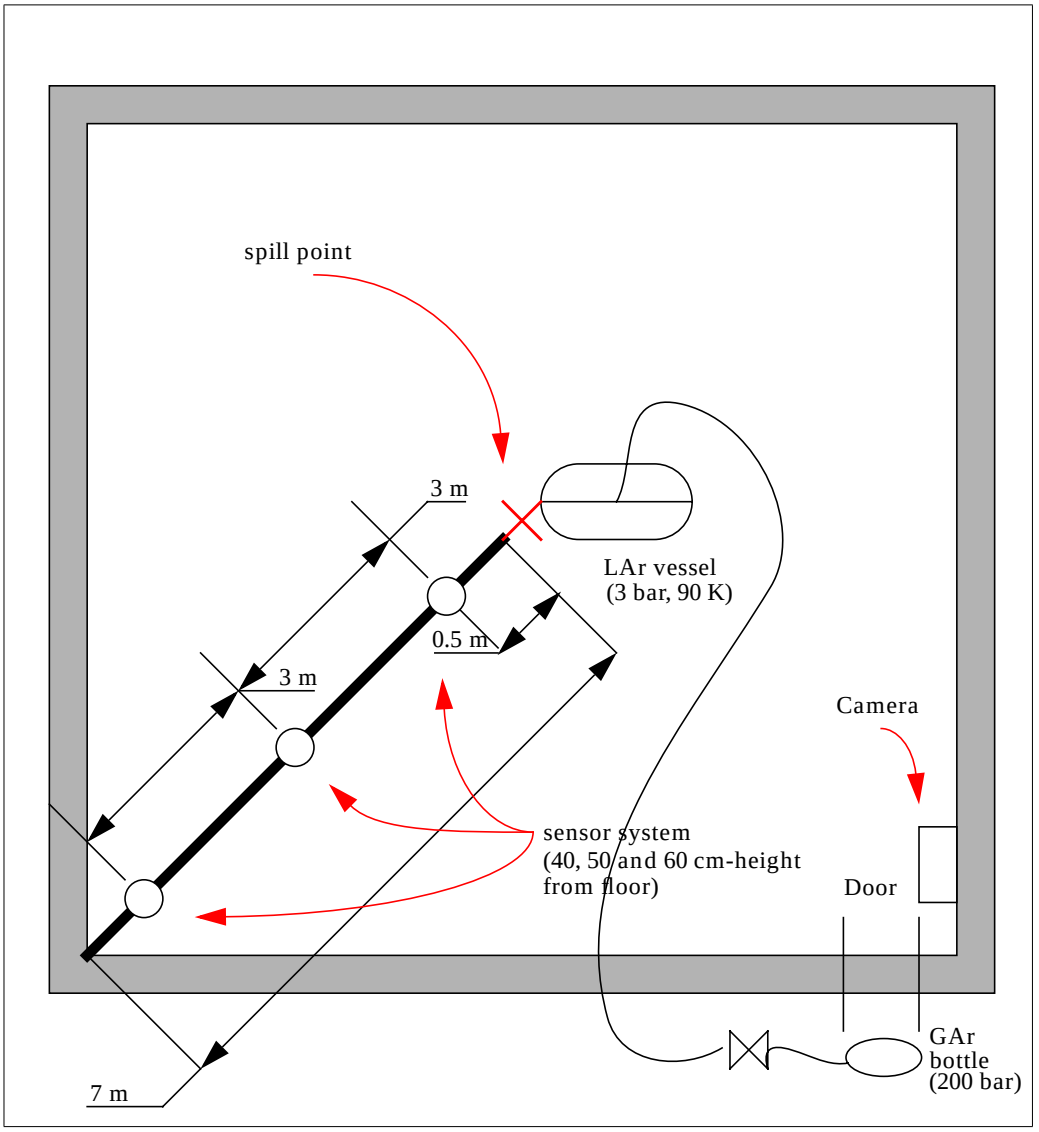

Figure 6 Experimental layout

The modelled 360 s-spill involves 60 l of liquid argon stored at 90 K and 3 bar abs. A stainless steel, horizontal cylindrical dewar (radius 0.325 m, length 1.5 m) was placed exactly in the middle of the room and connected with a 200 bar-argon bottle, by means of a stainless steel, valve-equipped tube inserted into the vessel (Fig. 6). The valve was used for regulating vessel pressure and kept it constant to 2 bar gauge (i.e. 3 bar abs.). The diameter of the spill tube is 18 mm. The ambient oxygen monitoring unit, based on the Detection and Neutralization System (SDN), which was initially designed and built for the LEP Experimental Areas, was installed in the test zones. It consisted of a set of paramagnetic sensors (three punctual sniffers at 50 cm above the floor and at different distances from the vessel, two linear[iv] sensors at 40 and 60 cm above the floor) that were placed at fixed points in the room and at different heights, in order to constantly monitor the evolution of the oxygen concentration.

[iv] i.e. mixing air taken at different points (at the same height) and measuring the average concentration.

The aim of our simulation is to reproduce as precisely as possible the values monitored by the sensors, and to verify if the argon cloud which is formed when the liquid touches the ground behaves in a similar way to reality.

Wherever possible, we tried to leave unchanged the set-up realized for the analysis of the accident scenarios in cavern UX15. In particular, the turbulence model and the spatial and temporal differencing methods remain the same as before. In order to obtain a better accuracy in the temperature field, two polynomial functions of temperature were introduced to express the specific heat of air and argon [J/kg/K]:

$$c_{p,\,air} = 0.001094*T^2 - 0.641065*T + 1099.122265$$

$$c_{p,\,Ar} = -5.817808*10^{-6}*T^3 + 0.004663*T^2 - 1.222364*T + 624.079536$$

Figure 7 shows the two curves.

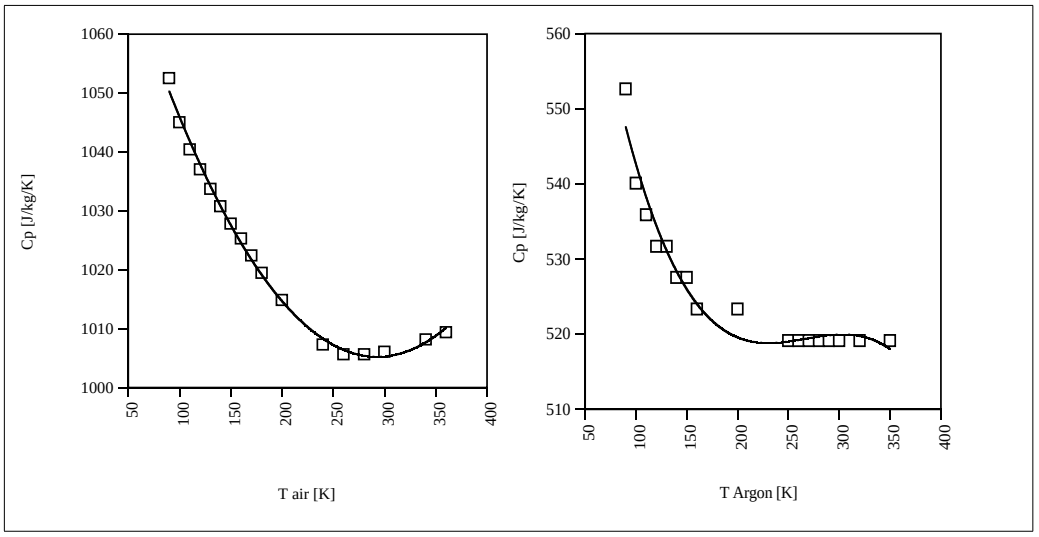

Figure 7 Specific heat of air and argon as a function of temperature (at 1 bar)

It is important to stress that the lack of some data (behaviour of internal pressure, liquid pool dimensions) and the conditions in which the experiment was realized (probable presence of a certain quantity of air-gas mixture inside the vessel) forced us to introduce a series of hypotheses and conservative assumptions while defining the model.

Both in the actual experiment and in the simulation, the rapid formation of a cloud of gaseous argon rising from a small pool was observed. As it is denser than air, it stratifies next to the floor and expands into the room. As soon as it reaches the external wall, the higher stratus changes direction and goes back towards the vessel, and the gas slowly tends to fill the hall. After the end of the spill, argon slowly begins to mix with air, so that the monitored O_2 concentration rises again. The performed simulation reproduces very closely the qualitative evolution of the phenomenon.

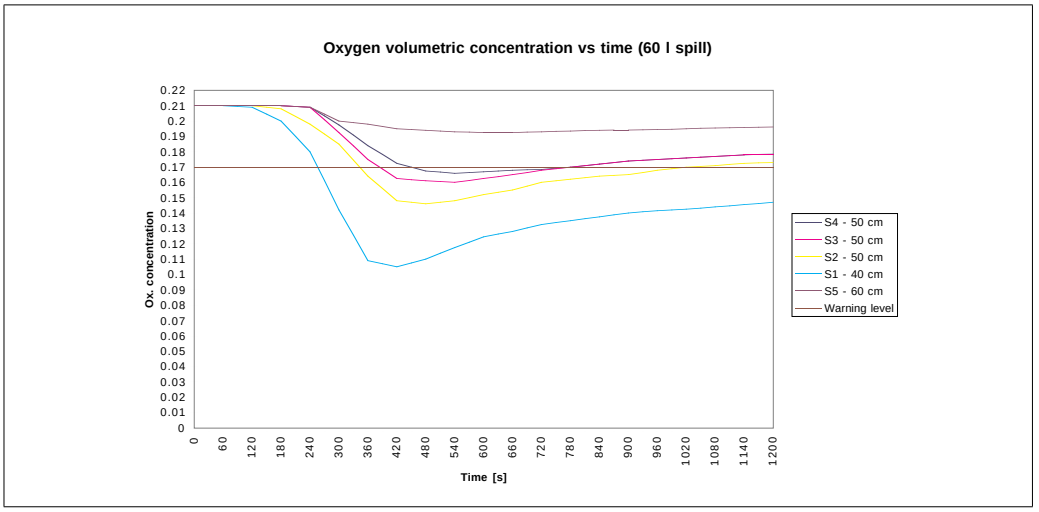

Figure 8 Evolution of oxygen concentration measured by sensors during the experiment

Figure 8 shows the evolution of oxygen concentration at the five sensors (sensors 1 and 5 are the linear ones) during the first 1200 seconds since the beginning of the spill. Note how the concentrations measured are lower for those sensors closer to the ground.

The experiment was reproduced using two different models (see below) and by means of a number of conservative hypotheses. One of the major assumptions is the pool dimension, which was not measured due to the fast and violent vaporization of argon. According to an existing movie of the spill and after brief discussion with the authors, we chose a radius of 10 cm.

- The *instant evaporation model* simply assumes that all the falling liquid argon vaporizes completely and instantaneously after having formed the pool. This means that the floor can provide enough heat for the cryogenic liquid evaporation for the whole duration of the spill. This is basically not true, because the falling argon cools the ground, but the assumption of instant and complete evaporation is conservative and not so far from reality.

The way in which we proceeded is very simple and is based on the conservation of mass (all of the fallen liquid is vaporized); this is shown in Fig. 9.

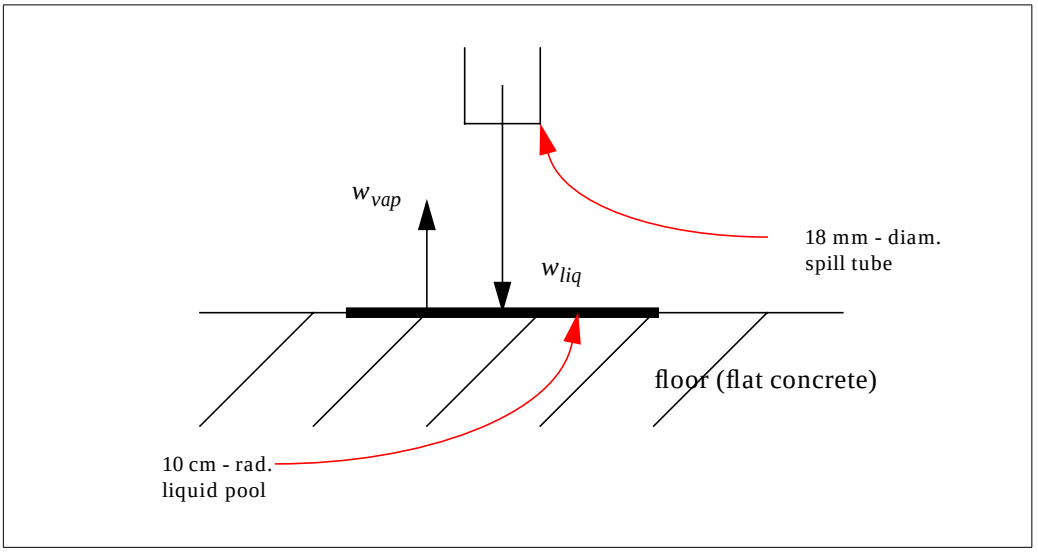

Figure 9 Pool evaporation scheme

We have[v] $w_{liq} = w_{vap}$. Note that as the evaporation flux varies in time, we'll have to recalculate the argon velocity at the inlet step by step.

- The second model is the *TNO simplified pool evaporation model* ([16] and Appendix 2). It is characterized by a set of less conservative - and probably more realistic - hypotheses than for the previous model, because it takes into account and models the heat exchange between the fluid and the ground. Here we are able to implement some characteristics of the flat concrete floor (non-permeability, density: ρ = 2200 kg/m^3, specific heat: c = 0.88 kJ/kg/K, thermal conductivity: k = 1.28 W/m/K). The ground characteristic parameter is $\alpha = \frac{k}{\rho c} = 0.0061 cm^2 s^{-1}$.

Figure 10 shows the oxygen concentration at the "virtual" sensors Star-CD allows us to implement.

[v] w indicates the argon mass flux in kg/s.

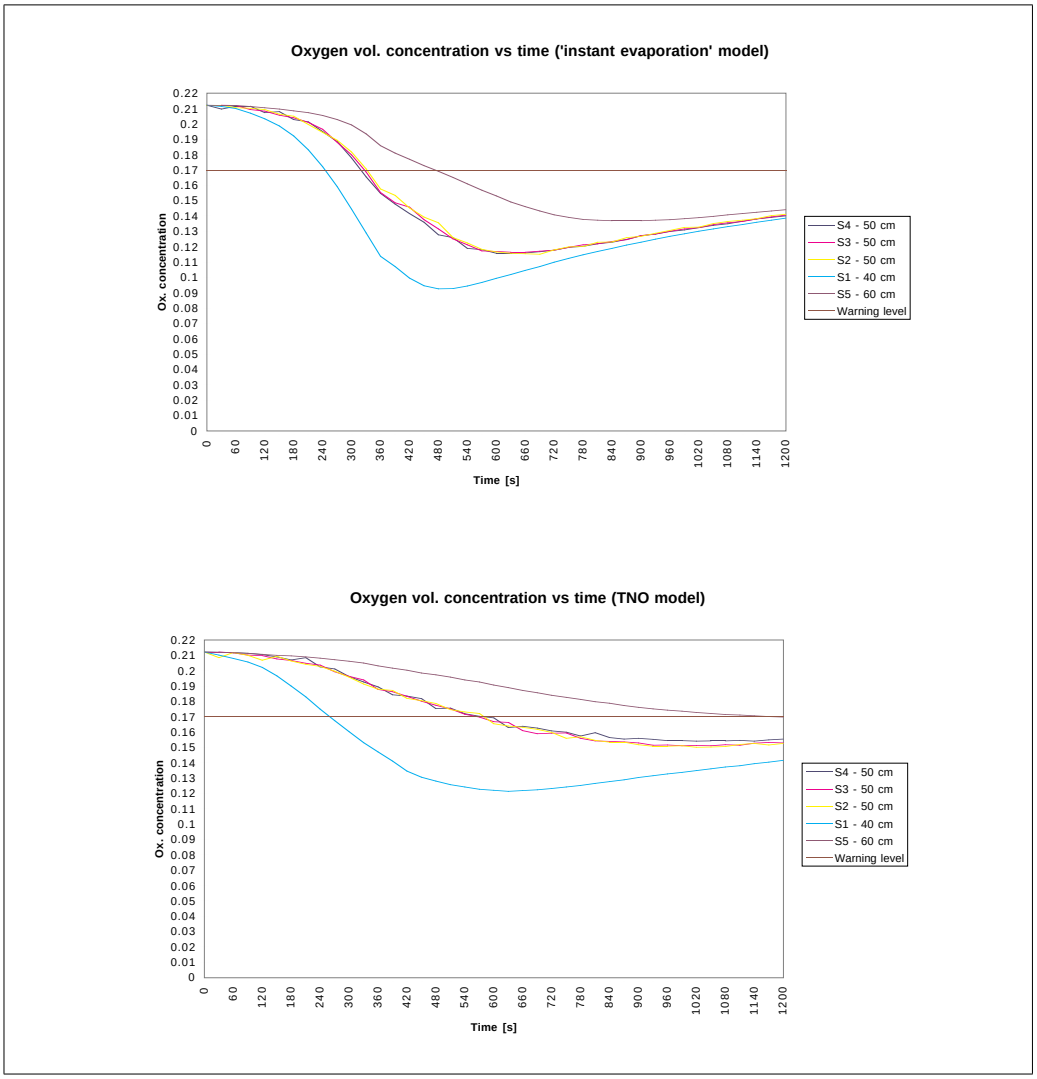

Figure 10 Simulated sensor surveys (above: “instant evaporation model”; below: “TNO model”)

As can be seen in comparison with Fig. 8, the situation is in fact conservative (i.e. worse than reality), the computed oxygen concentrations being below the measured values. In particular, we experienced a certain delay in the rise of the oxygen concentration after the end of the spill, especially at the highest sensors. Physically, the oxygen concentration rises faster in the sensors placed in lower regions because, after the end of the spill, even if the argon stratifies next to the floor, some not negligible mixing with air occurs, and a certain quantity of gas rises, thus the concentration increases in upper parts of the domain and decreases in others. This also happened in the experiment.

The agreement with experimental data is quite good, especially in the first part of the simulation, and all orders of magnitude are valid on the whole. A summary of the phenomena not taken into account is the following:

- the floor is not perfectly impermeable;
- part of the liquid is absorbed by the ground or forms a thin ice layer;

- during the 360 seconds-spill some air is also probably released from the pipe;
- the argon evaporation flux depends on the ground temperature and properties[vi];
- the assumed value for the pool radius does not result from a precise measuring.

Despite the relatively large number of assumptions made, the results are are found to be not far from reality. Moreover, the two computed flow fields and the oxygen concentration evolution at sensors are rather similar, in spite of the significantly different hypotheses and models. This means that most of our choices were not “critical”: the only factor that can significantly change the solution is the liquid pool dimension.

5 Safety recommendations

Given the modelled accidents, we are now able to draw up some general recommendations for personnel safety and the realization of an emergency plan:

- Access points and emergency exits in UX15 must be numerous and located in easily reachable zones, both at higher and lower levels. In particular, the access/exit to/from the barrel and end-caps must be made easy, because personnel working *inside* the detector will be liable to the highest risk in the case of an argon leak. An elevating platform will allow personnel to access different floors: as the contact with gas or liquid at cryogenic temperatures could hamper its mechanism, the evacuation should be planned without taking it into account;
- The number of people simultaneously working inside the detector and, in particular, close to or under the cryostat, must be minimized;
- The use of sensors and the isolation of damaged sections should permit adequate mitigation of a loss-of-argon accident, and won’t allow the situation to evolve into a more severe scenario. Redundant safety valves must be provided (already foreseen) and efforts must be made to avoid any “common cause failures”;
- Even if the modelled accidents point out the consequences of an argon loss, an estimation of the probabilities of occurrence of undesired events would allow a more correct risk evaluation;
- The evacuation plans for other experiments at CERN allow personnel to reach safe areas in less than three to four minutes. Some “biocells” (a sort of respirator foreseen in the experimental areas) with a 30 minutes duration will be available in UX15, but in case of an accident it is strongly recommended to look for an escape way rather than use them.

[vi] This was not taken into account only in the first model.

Further, in order to get more precise information about the argon evaporation flux and about argon spill accidents in the ATLAS experimental cavern, and as the comparison of the experiment with the computer simulation was satisfying, it seems necessary to realize a new test. The main physical properties should be carefully monitored, the initial pool dimension measured as well as its changes in time, and the characteristics of the ATLAS cryostat should be reproduced in more details.

6 Conclusions

The main difficulties when performing finite-element or finite-volume analysis are to draw a geometry which reasonably simulates the environmental domain, to get *numeric convergence* in acceptable times and to show that results are *credible* (the credibility of the results is not always a consequence of the convergence of the method). Most times, the computational times govern and limit the choices.

This task presented the additional complication of modelling the sudden entrance of a new chemical species in the domain, and a high temperature gradient (~200 K) in respect to the surrounding atmosphere. Besides, this gradient was concentrated in a very small zone and no steady solution was possible as the situation was expected to evolve very rapidly.

We think that the geometries we used are a good approximation of reality, and the fact that the computed fields do not change much even after adding two muon chamber layers seems to confirm that the geometry is acceptable. We tried to implement the largest number of physical models the code could sustain in order to get as accurate results as possible, the cost being long waiting times. Very high memory is required for such simulations, especially when, like in our case, all the models are *transient* and not *steady-state*.

Internal convergence was validated by the code both for spatial and time differencing. This means that the set-up, and all the hypotheses, boundary and initial conditions were well defined and coherent. In order to prove that the results are credible, we used two methods:

- we performed a sensibility study on the mesh, refining it in the most “critical” points (i.e. where the steepest temperature / velocity gradients are located) until the computed flow fields do not significantly change after adding more cells. This is in fact the best way of proving overall convergence and the accuracy of the results;
- we simulated an actual argon spill test using the same methods as in the ATLAS simulations and showed that the computed flow fields respect experimental results and measurements, and are of the same order of magnitude.

After having verified that all boundaries and models were correctly specified, and having proved that the model succeeded in all internal tests

and validations, we could reasonably state that the final results were encouraging and managed to give a valid view of the phenomena, both globally and locally.

The results of this work were also officially presented at the “High Energy Physics Laboratory Technical Safety Forum” (Desy, Germany, 5th - 7th October 1999).

Acknowledgements

We thank W. Weingarten (TIS/GS) for his support throughout the year, as well as Prof. G. Del Tin (Politecnico di Torino, Italy) for his supervision.

Thanks also to ASSTP (Association for the Scientific and Technological Development of Piemonte) for the financial support and for the trust in our work.

Special thanks to R. Clayton (Computational Dynamics, London, England), C. Wolf (Computational Dynamics, Paris, France) and Prof. E. Cafaro (Politecnico di Torino, Italy) for their help with the software. Thanks to S. Buono (SL/ETT), G. Peon (ST/CV) and A. Catinaccio (EP/TA1) for their much valued advice, and thanks also to J. Nebout and C. Gregory (EST/LEA) for their kind availability and explanations about the LAr spill tests.

Appendix 1 - Methodology

For the realization of all of our simulations we made use of a code named *Star-CD* ([14],[15]). It uses the *Finite-Volume method* (see also [17], [18]) in solving complex systems of strongly coupled equations, in steady-state or transient regime. The results are presented as a series of graphics showing the behaviour of different physical properties in the considered domain.

The user is allowed to create two- and three-dimensional geometries and meshes; the implementation of a number of turbulence models as well as many different spatial and temporal differencing techniques is also possible.

Basically, this method carries out the analysis (by means of the numerical algorithm *PISO*) in the following steps:

- formal integration of the governing equations of fluid flow over all the (finite) control volumes of the solution domain.
- discretisation of these equations by substituting a variety of finite-difference-type approximations for the terms in the integrated equation representing flow process as convection, diffusion and sources. This converts the integral equations into a system of algebraic equations.
- solution of the algebraic equations by an iterative method.

In our simulations we have always made use of a two-dimensional geometry, and we'll refer to the section of cavern UX15 corresponding to the rupture and the release of a certain quantity of argon (Fig. 1).

Using the Finite-Volume method the approximated solutions satisfy a local conservation law on each volume. In other words, if the method is applied to equations written in their "conservative" form, the discrete solution will also have the same property. This is *not* true in other methods such as the Finite-Element one.

Referring to our specific situation and to the mathematical formulation of the program, the seven fundamental equations Star-CD solves for each cell and each time step (after proper discretisation and decoupling) are, in their general form:

$$\frac{1}{\sqrt{g}}\frac{\partial}{\partial t}(\rho\sqrt{g}) + \frac{\partial}{\partial x_j}(\rho\tilde{u}_j) = s_m \quad \text{(Mass conservation)}$$

$$\frac{1}{\sqrt{g}}\frac{\partial}{\partial t}(\rho\sqrt{g}u_i) + \frac{\partial}{\partial x_j}(\rho\tilde{u}_j u_i - \tau_{ij}) = -\frac{\partial p}{\partial x_i} + s_i \quad \text{(Momentum conservation, 2 equations)}$$

$$\frac{1}{\sqrt{g}}\frac{\partial}{\partial t}(\rho\sqrt{g}h_t) + \frac{\partial}{\partial x_j}\left(\rho\tilde{u}_j h_t - F_{h_t,\,j}\right) = \frac{1}{\sqrt{g}}\frac{\partial}{\partial t}(\sqrt{g}p) + \tilde{u}_j\frac{\partial p}{\partial x_j} +$$

$$+ \tau_{ij}\frac{\partial u_i}{\partial x_j} + s_h - \sum_m m_m H_m s_{c,\,m} \quad \text{(Energy conservation - enthalpic form)}$$

$$\frac{1}{\sqrt{g}}\frac{\partial}{\partial t}(\rho\sqrt{g}m_m) + \frac{\partial}{\partial x_j}(\rho\tilde{u}_j m_m - F_{m,\,j}) = s_m \quad \text{(Transport equation for the second chemical species)}$$

$$\frac{1}{\sqrt{g}}\frac{\partial}{\partial t}(\rho\sqrt{g}K) + \frac{\partial}{\partial x_j}\left(\rho\tilde{u}_j K - \frac{\mu_{eff}}{\sigma_k}\frac{\partial K}{\partial x_j}\right) =$$

$$= \mu_t(P + P_B) - \rho\varepsilon - \frac{2}{3}\left(\mu_t\frac{\partial u_i}{\partial x_i} + \rho K\right)\frac{\partial u_i}{\partial x_i} \quad \text{(Turbulent kinetic energy)}$$

$$\frac{1}{\sqrt{g}}\frac{\partial}{\partial t}(\rho\sqrt{g}\varepsilon) + \frac{\partial}{\partial x_j}\left(\rho\tilde{u}_j\varepsilon - \frac{\mu_{eff}}{\sigma_\varepsilon}\frac{\partial\varepsilon}{\partial x_j}\right) = \frac{\varepsilon}{K}[\mu_t(C_{\varepsilon 1}P + C_{\varepsilon 3}P_B) +$$

$$-\frac{2}{3}\left(\mu_t\frac{\partial u_i}{\partial x_i} + \rho K\right)\frac{\partial u_i}{\partial x_i}] - C_{\varepsilon 2}\rho\frac{\varepsilon^2}{K} + C_{\varepsilon 4}\rho\varepsilon\frac{\partial u_i}{\partial x_i} - \frac{C_\mu\eta^3\left(1 - \frac{\eta}{\eta_0}\right)}{1 + \beta'\eta^3}\frac{\rho\varepsilon^2}{K}$$

(Dissipation rate for turbulent kinetic energy)

where:

- t = time;
- x_i = Cartesian coordinate (i = 1, 2, 3);
- u_i = absolute fluid velocity component in direction x_i;
- $\tilde{u}_i = u_j - u_{cj}$, relative velocity between fluid and local (moving) coordinate frame that moves with velocity u_{cj};
- p = piezometric pressure = $p_s - \rho_0 g_m x_m$, where p_s is the static pressure, ρ_0 is the reference density, g_m is the gravitational field component and x_m is the coordinate from a datum, where ρ_0 is defined;
- ρ = density;
- $\tau_{ij} = 2\mu s_{ij} - \frac{2}{3}\mu\frac{\partial u_k}{\partial x_k}\delta_{ij} - \bar{\rho}\overline{u'_i u'_j}$ = stress tensor components for Newtonian fluids in turbulent flows, where all the dependent variables assume their average values; u' is the fluctuation about the average

velocity and the overbar denotes the averaging process; δ_{ij} is the so-called "Kronecker delta", equal to unity when $i = j$ and zero if $i \neq j$. The term on the right-hand side represents the additional Reynolds stresses due to turbulent motion (see also next paragraph);

- $s_{ij} = \frac{1}{2}\left(\frac{\partial u_i}{\partial x_j} + \frac{\partial u_j}{\partial x_i}\right)$ = rate of strain tensor;
- s_m = mass source;
- $s_i = g_i(\rho - \rho_0)$ = buoyant forces, essentially the only contribution to momentum source components; here g_i is the gravitational acceleration in direction x_i;
- $\sqrt{g}$ = determinant of metric tensor;
- m_m = mass fraction of mixture component *m;*
- H_m = heat of formation of constituent *m;*
- $h_t = \tilde{c}_p T - c_p^0 T_0$ =thermal enthalpy, with $\tilde{c}_p$ = mean constant-pressure specific heat at temperature *T*, and c_p^0 = reference specific heat at temperature T_0;
- s_h = energy source;
- $s_{c,m} = s_m$ = rate of production or consumption of species *m* due to chemical reaction (always = 0 for us, as argon does not react with anything);
- $F_{h_t, j} = k\frac{\partial T}{\partial x_j} - \bar{\rho}\overline{u'_j h'} + \sum_m h_{m,t}\rho D_m \frac{\partial m_m}{\partial x_j}$ = diffusion energy flux in direction x_j in turbulent flow, where the middle term containing static enthalpy ($h_{m,t}$) or thermal enthalpy fluctuations (h'_t) represents the turbulent diffusion flux of energy, *k* is the thermal conductivity and D_m is the molecular diffusivity of constituent *m;*
- $F_{m,j} = \rho D_m \frac{\partial m_m}{\partial x_j} - \bar{\rho}\overline{u'_j m'_m}$ = diffusion flux component; the right-hand term, containing the concentration fluctuation m'_m, represents the turbulent mass flux;

Note: $\frac{\partial}{\partial x_j}(\rho u_j) = \frac{\partial}{\partial x}(\rho u) + \frac{\partial}{\partial y}(\rho v) + \frac{\partial}{\partial yz}(\rho w) = \nabla\bullet(\rho\vec{u}) = div(\rho\vec{u})$.

From these equations the values of the dependent variables ρ, *u*, *v*, *h*, m_{Ar}, *K*, ε are obtained; nevertheless we need further details about the turbulence.

The used turbulent model, corresponding to the last two equations, is the so-called *Renormalization Group (RNG) K*-ε. It allows us to take into account,

by means of proper options, *buoyancy* (i.e. the influence of natural convection) and fluid compressibility (gaseous argon at variable temperature). The random nature of a turbulent flow precludes computations based on a complete description of the motion of all the fluid particles. We must re-define the velocity in this way:

$$\vec{u}(t) \rightarrow \vec{U}(t) = \vec{u} + \vec{u}'(t) \quad ,$$

where the velocity is broken down into a steady mean value u with a fluctuating component u' superimposed on it. For the last two equations the symbology has the following meaning:

- $-\bar{\rho}\overline{u'_i u'_j} = 2\mu_t s_{ij} - \frac{2}{3}\left(\mu_t \frac{\partial u_k}{\partial x_k} + \rho K\right)\delta_{ij}$, $\bar{\rho}\overline{u'_j h'} = -\frac{\mu_t}{\sigma_{h,t}}\frac{\partial h}{\partial x_j}$,
- $\bar{\rho}\overline{u'_j m'_m} = -\frac{\mu_t}{\sigma_{m,t}}\frac{\partial m}{\partial x_j}, K = \frac{1}{2}(u'^2 + v'^2 + w'^2)$ and $\mu_t = f_\mu \frac{C_\mu \rho K^2}{\varepsilon}$,

where $\sigma_{h,t}$ and $\sigma_{m,t}$ are the turbulent Prandtl and Schmidt numbers, respectively. Both these two numbers and C_μ and f_μ are empirical coefficients, usually constant,

and:

- $\mu_{eff} = \mu + \mu_t$; μ is the molecular dynamic fluid viscosity, $\mu_t = f_\mu \frac{C_\mu \rho K^2}{\varepsilon}$ is the turbulent viscosity (C_μ and f_μ are empirical coefficients);
- $P = 2 s_{ij} \frac{\partial u_i}{\partial x_j}$ and $P_B = -\frac{g_i}{\sigma_{h,t}} \frac{1}{\rho}\frac{\partial \rho}{\partial x_i}$;
- $\eta = S\frac{K}{\varepsilon}$ and $S = \sqrt{2 s_{ij} s_{ij}}$.

The remaining coefficients are empirical and their value is set for default by Star-CD.

The mixture density is calculated by means of a special ideal gas law taking into account the simultaneous presence of more than one chemical species, while other properties (specific heat, thermal conductivity, molecular viscosity) are averaged on the basis of the weight concentration of argon and air and of the reference values of such properties.

The assumed property values for argon are ([11]):

Property/Parameter	*Value/Setting*
Influence	Active
Molecular weight	39.94 g / mol
Density (1 bar, 90 K), ρ	5.3375 kg / m^3 [a]
Thermal exp. coefficient, β	0.0111 K^{-1} [b]
Specific heat (1 bar, 90 K)	552.658 J / kg / K
Thermal conductivity (1 bar, 90 K), *k*	0.006142 W / m / K
Molecular viscosity (1 bar, 90 K), μ	7.45*10^{-6} Pa*s
Initial concentration	0
Molecular diffusivity, *D*	3.004*10^{-5} m^2 / s [c]
Turbulent Schmidt number, $\sigma_{m,t}$	0.9 [d]

a. Calculated by means of the ideal gas law, with $R^* = 208.17$ J / kg / K. In the last simulation we'll take the tabled value ([11]) of 5.5075 kg / m^3.
b. Calculated by means of the well-known formula for ideal gases $\beta = 1/T$, with $T = 90$ K.
c. Default value from Star-CD database.
d. Default value from Star-CD database.

After integration onto the control volume and a rather large amount of mathematics, the final form of the continuity equation is:

$$\frac{(\rho V)_P^{n+1} - (\rho V)_P^n}{\delta t} + \sum F_j^{n+1} = 0 \qquad (1)$$

while for any other dependent variable ϕ the most compact form for the general FV discrete equation is:

$$A_P \phi_P^{n+1} = \sum_m A_m \phi_m^{n+1} + s_1 + B_P \phi_P^n \qquad (2)$$

where:

- *n* and *n+1* represent two subsequent time steps;
- A_m represents the effects of convection and diffusion;
- the summation is over all neighbour nodes used in the flux discretisation;
- $B_P = \frac{(\rho V)_P^n}{\delta t}$;
- $A_P = \sum_m A_m + s_2 + B_P$.

There are equations like (1) and (2) for every computational cell (suitably modified according to the particular conditions and boundaries), and there are as many equations as dependent variables.

We won't describe in detail all the differencing methods, for which the reader can refer to [14] or [17]. For the spatial discretisation we used, whenever model complexity and computational time made it possible, the second-order scheme MARS for all variables except density (for which we used the "Central Differencing" second-order method). Otherwise, we made use of the first-order Upwind (UD) method. For the temporal differencing - all our simulations represent transient models - we used a Fully-Implicit scheme, which is unconditionally stable even if it is more computationally expensive than the Explicit or Crank-Nicolson methods. Finally, we implemented a specific set of initial and boundary conditions for each modelled problem (for a compressible, viscous, unsteady flow[vii]):

Initial conditions:

- Everywhere in the solution region ρ, $\vec{u}$, T, K, ε and chemical species concentration must be given at time t = 0.

Boundary conditions:

- Solid walls: no-slip condition $\vec{u} = \overrightarrow{u_w}$; $T = T_w$ (fixed temperature) or $k\frac{\partial T}{\partial n} = -q_w$ (fixed heat flux).
- Fluid inlet boundaries: ρ, $\vec{u}$, T, K, ε and chemical species concentration must be known as a function of position. In particular, fluid (air or argon) velocity is calculated by means of the formula:

$$v = \frac{Q}{3600 \cdot l_k L}$$

where Q is the volumetric flow at inlet (in m^3/h), l_k is the section of the inlet and L is the length of the cavern. This is justified by the fact that as our model is two-dimensional we are forced to calculate an "equivalent" source term.

- Fluid outlet boundaries (tangential): $\mu\frac{\partial u_t}{\partial n} = F_t$
- Fluid outlet boundaries (normal): $-p + \mu\frac{\partial u_n}{\partial n} = F_n$
- Symmetry boundaries: $\frac{\partial \phi}{\partial n} = 0$, where ϕ is any dependent variable.

[vii] Suffices *n* and *t* here indicate directions normal (outward) and tangential to the boundary respectively and *F* is the given surface stress.

Appendix 2 - The TNO simplified model for pool evaporation

When a liquefied gas comes into contact with the floor, an immediate heat transfer takes place between the cold liquid and the relatively warm ground. The TNO model ([16]) we used determines the resulting one-dimensional heat flow by means of the Fourier equation for the cooling of a half-endless medium. The Fourier equation states (if z is the only spatial coordinate and is 0 at floor level):

$$\frac{\partial T}{\partial t} = \alpha \frac{\partial^2 T}{\partial z^2} \tag{3}$$

with the initial condition:

- $T(z, t = 0) = T_s = 293$ K for $z \geq 0$

and the boundary conditions:

- $T(z = 0, t) = T_k = 90$ K and
- $\lim_{z \to \infty} T(z, t) = T_s = 293K$, both for $t > 0$.

The solution of equation (3) is the following:

$$T(z, t) = T_k + (T_s - T_k) erf\left[\frac{z}{2\sqrt{\alpha t}}\right] \tag{4}$$

where the (mathematical) error-function is given by:

$$erf(x) = \frac{2}{\sqrt{\pi}} \int_0^x e^{-s^2} ds \tag{5}$$

For the heat-flow through the area $z = 0$ the following applies:

$$q_s = -k\left(\frac{dT}{dz}\right)_{z=0} = \frac{k(T_s - T_k)}{\sqrt{\pi \alpha t}} = e h_v t^{-\frac{1}{2}} \tag{6}$$

corresponding with the evaporation flux:

$$\dot{m}''_s = e t^{-\frac{1}{2}} \tag{7}$$

where $h_v = 160.81$ kJ/kg is the heat of vaporization of argon and

$$e = \frac{k(T_s - T_k)}{h_v\sqrt{\pi\alpha}} = 1.1213.$$

If the heat necessary for the evaporation of a liquefied cooled gas is assumed equal to the heat-flow from the floor moistened by the liquid, the evaporation flux of our liquefied cooled gas on a non-permeable ground can be calculated by means of (7).

It comes out that the evaporation flux strongly decreases with time, as we said before, so this model seems to be more realistic than the previous one. Again, we have to re-define the argon inlet more than once in order to reproduce the variable evaporation flux (and consequently the variable velocity of the rising gas). We subdivided the 1200 seconds in various intervals and taking arithmetical averaged-values of the evaporation flux:

$$\dot{m}''_s = \frac{\dot{m}''_s(t_1) + \dot{m}''_s(t_2)}{2}.$$

Wherever possible, we kept the control parameters unchanged in respect to the accident simulations. In particular, nothing changes in argon specification, spatial and temporal discretization (the time step does not exceed 0.05 - 0.1 seconds) and turbulence modelling.

References

1 **ATLAS - Technical proposal for a general-purpose pp experiment at the Large Hadron Collider at CERN**
CERN / LHcc / 94-43, 1994

2 **Requirements and design criteria for ATLAS**
M. Fernandez-Bosman - 1997 / 1998 Academic Training Program

3 **Overview of the ATLAS electromagnetic calorimeter**
W. Bonivento - LAL 98-102, 1998

4 **The ATLAS detector for the LHC**
Proceedings of the XXVI International Conference on High Energy Physics, vol. II, Dallas (Texas), 1992

5 **ATLAS liquid Argon calorimeter - Technical Design Report**
CERN / LHCC / 96-41, 1996

6 **The use of cryogenic fluids**
TIS-IS-47, 1998

7 **Preliminary Risk Analysis of the ATLAS experiment cryogenic systems**
Principia-EQE - Report n. 296-03-R-04, 1998

8 **Liquid Argon spill tests**
C. R. Gregory, J. Nebout - AT-XA / 01N / CG / JN, May 1994

9 **Lezioni di Termocinetica**
B. Panella - Cooperativa Libraria Universitaria Torinese ed.

10 **Analisi di sicurezza di impianti a rischio rilevante - modelli per lo studio dei termini di sorgente**
L. Prezioso, A. Carpignano - PT DE 388 / IN, May 1995

11 **Encyclopedie des gaz**
Elsevier / L'Air Liquide, 1976

12 **Argon spill in the hall of ATLAS experiment**
G. Peon, L. Gustavsson - CERN Technical Note ST-98-038, 1998

13 **Evaluation of unforeseen liquid Argon spill in ATLAS**
2nd Safety Forum meeting for LHC experiments, TIS Web pages

14 **Star-CD - Methodology (version 3.05)**
Computational Dynamics, 1998

15 **Star-CD - User Guide (version 3.05)**
Computational Dynamics, 1998

16 **Methods for the calculations of physical effects**
CPR 14E - Committee for the Prevention of Disasters - TNO, second edition, 1992

17 **An introduction to Computational Fluid Dynamics - The Finite-Volume Method**
H. K. Versteeg, W. Malalasekera - Longman Scientific&Technical, 1995

18 **Fluid Dynamics and Heat Transfer**
G. Knudsen, D. L. Katz - McGraw-Hill Book Company, INC., 1958